Electronic Supplementary Material (ESI) for Lab on a Chip.

Supporting Information

Dual-modality microfluidic biosensors based on nanoengineered mesoporous graphene hydrogels

Nawab Singh[a], Md. Azahar Ali[b] Prabhakar Rai[c], Inayathullah Ghori[a,d], Ashutosh Sharma[c], B. D. Malhotra[e]*, and Renu John[a]*

[a]Department of Biomedical Engineering, Indian Institute of Technology Hyderabad, 502285 Telangana, India.
[b]Department of Aerospace and Mechanical Engineering, University of Notre Dame, Notre Dame, Indiana- 46556, USA.
[c]Department of Chemical Engineering, Indian Institute of Technology Kanpur, Kanpur, 208016, India.
[d]Department of Cardiology, Kamineni Koti Hospital, Hyderabad-500001, Telangana, India.
[e]Department of Biotechnology, Delhi Technological University, Shahbad Daulatpur, Main Bawana Road, Delhi-110042, India.

***Corresponding authors:** renujohn@iith.ac.in*, Ph: +91-40-23016097, bansi.malhotra@gmail.com*

Chemicals and reagents

Graphite powder flakes (45 µm, > 99.99, wt %), L-cysteine, bovine serum albumin (BSA), were procured from Sigma Aldrich, USA. Thionyl chloride, Tetrahydrofuran (THF), 1-hydroxy-2,5-pyrrolidinedione (NHS), and 1-(3-(dimethyl amino)-propyl)-3-ethylcarbodiimide (EDC) were purchased from Sigma Aldrich, USA. The polydimethylsiloxane (PDMS) and negative-tone SU 8 2050 photoresist (PR) was purchased from Microchem (Newton, MA), USA. Human cMb antigen and mouse antibodies (monoclonal), cMb were purchased from Abcam, USA.

Device fabrication

A chemical etching resistance mask was applied onto Au coated glass substrate to make microelectrode patterned with a size of 3mm × 2cm via wet etching. The Au substrate was immersed in an etching solution of (1:3, HNO_3/HCL) for 120 s at 25 °C after which the substrate was dipped in DI water and the mask was unwrapped from the substrate. Further, the working electrode was treated with solution of (3:1, H_2SO_4/H_2O_2) for 5 min and was washed with DI water. For self-assembled monolayer of Cys-RGO hydrogel solution onto Au working electrode surface, Au electrode was dipped in Cys-RGO hydrogel solution for 12 h at room temperature (25 ^{0}C) in a closed chamber. The thiol group (−SH) of cysteine got attached to the Au surface via electrostatic interactions owing to essential property of Au indicating greater affinity towards Au surface. To fabricate the reference electrode, 500 nm thickness of Ag layer was depositted on the glass substrate via direct current DC sputtering. The Au electrode was treated with 0.1 M potassium chloride solution for 60 s to form Ag/AgCl reference electrode while the bare Au electrode performed as a counter electrode.

The PDMS microchannel was fabricated using soft lithography technique. For this purpose, SU-8 negative photoresist was spin coated on glass substrate with around 200 µm thick layer after that glass substrate was heated on hot plate at 95 °C for 40 min and UV exposed through mask. The substrate was heated once more for 15 min at 100 °C for post exposure bake and was developed to eliminate unexposed portion in order to form the master. This master was cleaned by isopropyl alcohol. The mixture of pre-polymer and silicon elastomer (10:1), was poured on top of the master after which the cured PDMS slab was peeled off from the master. The PDMS microchannel (height and width, 200 µm) was bonded with decorated Cys-RGO/Au electrode via plasma cure and was connected to the single inlet outlet and through the connectors. The stepwise illustration of microfluidic channels fabrication and bonding with sensor electrode is shown in (Fig. 2).

Instrumentation

The crystalline properties of the synthesized RGO and Cys-RGO composite were examined by X-ray diffraction (XRD) using a PANalytical, Germany and Raman spectroscopy. Fourier transform infrared spectroscopy (FT-IR, PerkinElmer, Model 2000) was used to investigate the conjugation of RGO and Cys-RGO with cMAb. Surface area and pore size calculated by Quanta Chrome and X-ray photoelectron spectroscopy (XPS; PHI 5000 Versa Prob II, FEI Inc.) was used to study the surface properties of functionalized material. The morphology and structure of the RGO and Cys-RGO composite were determined by field emission scanning electron microscope (FESEM; ZEISS Supra 40VP, Germany) and transmission electron microscope (TEM; FEI Titan G2 60-300). The interaction of antigen-antibody and electrochemical response of the microfluidic chip for cMb quantification were conducted using SPR and an Autolab (Model AUT-86000), respectively.

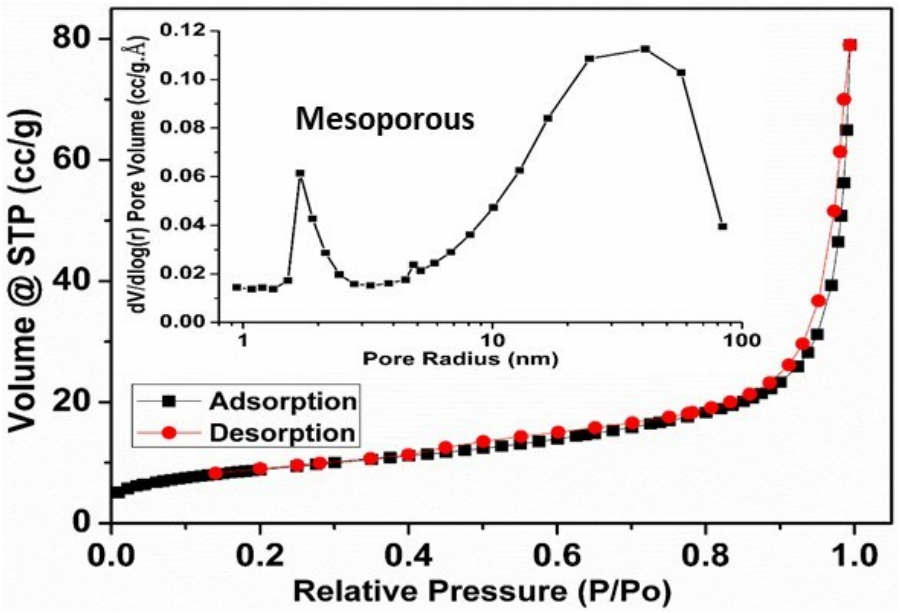

Fig.S1 BET characterization: Nitrogen adsorption-desorption isotherm of Cys-RGO hydrogel. Inset: pore size distribution graph.

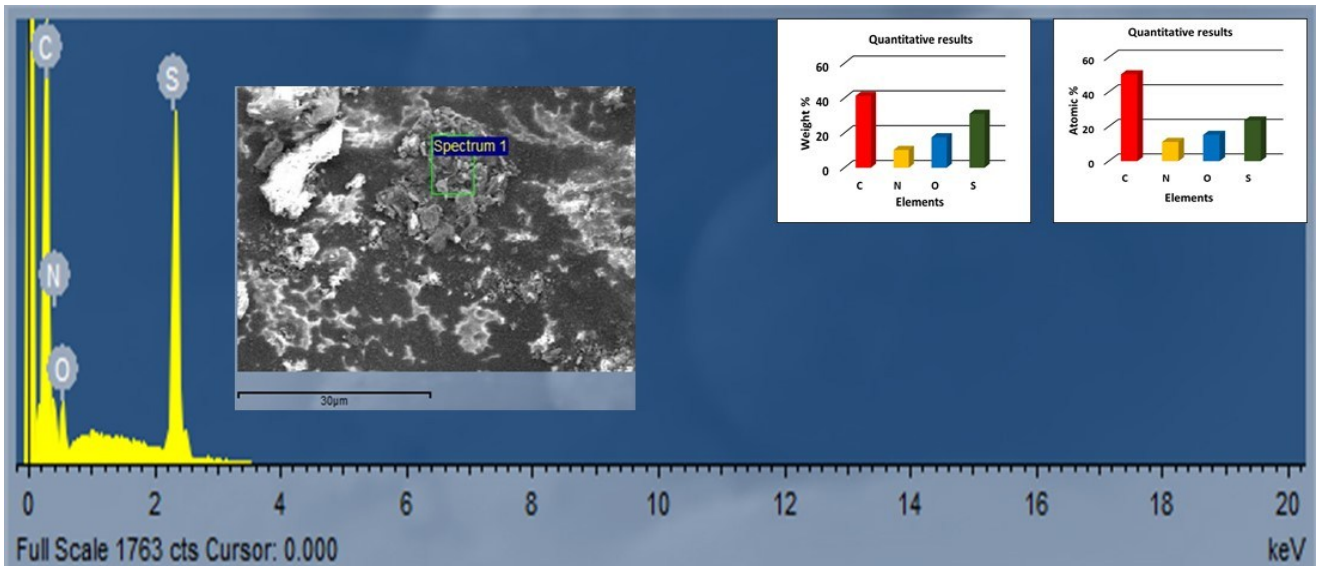

Fig.S2 Energy-dispersive X-ray (EDX) of Cys-RGO. Inset shows the presence of atomic and weight percentage of C, N, O and S in Cys-RGO hydrogel.

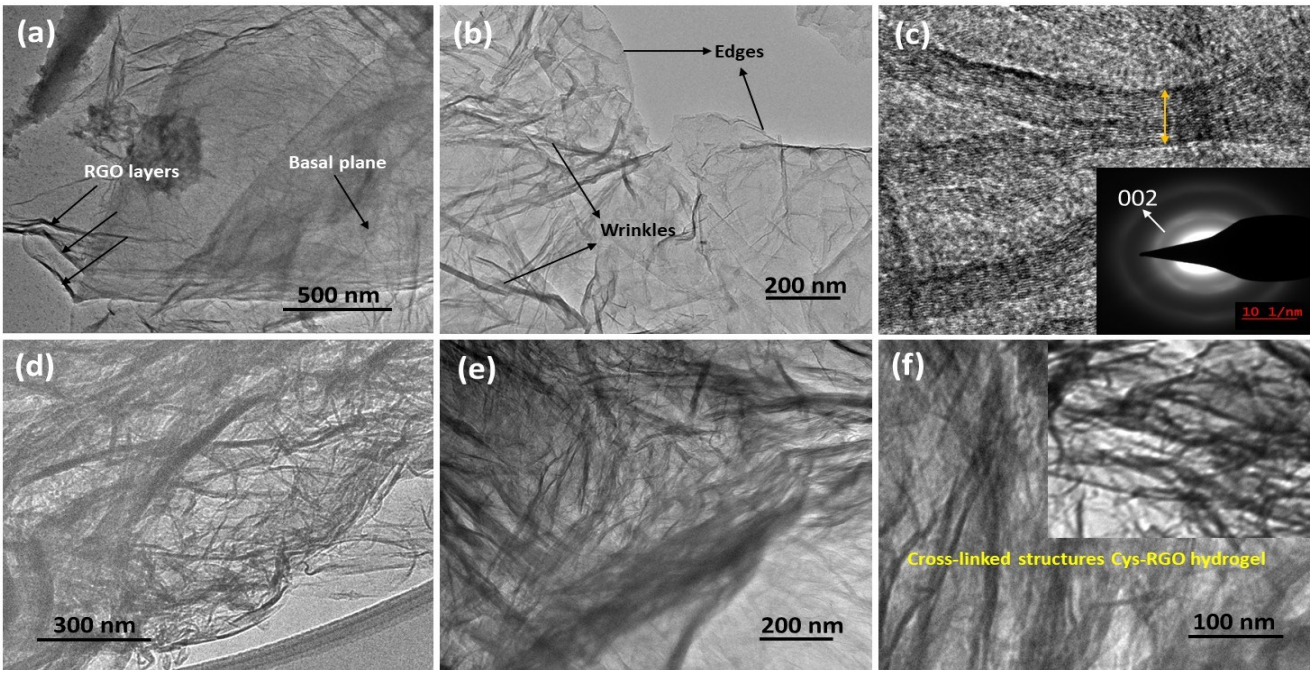

Fig. S3. TEM characterization of the RGO and Cys-RGO hydrogel. (a and b) TEM images of RGO nanosheets. (d) Atomic-scale image of RGO nanosheet. Inset: SAED pattern. (d, e and f) images of Cys-RGO hydrogel.

SPR measurements

The response signal of antigen-antibodies interaction was recorded on the cMAb/Cys-RGO/Au microfluidic biosensor surface (Fig. 9c). The different concentrations of cMb were run into the microfluidic biosensor surface. During the interaction of each cMb concentration, the first 120 s represented the baseline after which the cMb sample solution was injected and enabled it to interact with the cMAb/Cys-RGO/Au biosensor for the subsequent 360 s (association phase). At the end of the association, the cMAb/Cys-RGO/Au biosensor was washed with PBS and the SPR signal was recorded. The value of SPR angle increased when the interaction process was completed. The cMAb/Cys-RGO/Au biosensor was regenerated with PBS solution of pH 7.4 after interaction of each cMb concentration.

Electrochemical characterization

The electrochemical anodic peak current of the fabricated electrodes (RGO, Cys, Cys-RGO and cMAb/Cys-RGO bioelectrode) was measured in the presence of 50 milli molar (mM) PBS (pH 7.4) containing 5 mM ferro-ferricynide as redox electrolyte at 20 mV/s scan rate (Fig. 7a). Increasing the scan rate of cyclic voltammetry (CV) measurements of different electrodes, the peak currents of both anodic (I_{pa}) and cathodic (I_{pc}) increased alongwith the linear shift of the peak potential $(\Delta E_p = E_{pa} - E_{pc})$. Thus, the RGO, Cys, Cys-RGO electrodes and cMAb/Cys-RGO bioelectrode showed diffusion controlled processes. The surface diffusion coefficient (D) of these electrodes in ferro-ferricyanide electrolyte solution was calculated using the Randles–Sevcik Eq. S1[1].

$$I_p = k\, n^{3/2} A \sqrt{D}\; C \sqrt{v} \qquad \text{(S1)}$$

where k, n, A, D, C v and I_p are the constant, the number of electrons appearing in half-reaction for the redox couple (n = 1), the area of the electrode (0.006 cm^2), the diffusion coefficient, the concentration of the electrolyte (5 mM), the CV measured scan rate (20 mV s^{-1}) and the anodic and cathodic peak current, respectively.

The surface concentration of the electrode owing to the redox conversion can be calculated using Brown-Anson model as given Eq. S2[1,2].

$$I_p = \mathrm{I}^{*} A\, v\, n^2 F^2 (4RT)^{-1} \qquad \text{(S2)}$$

where I^{*}, A, v, n, F, R and T are the electrode surface concentration, the area of the electrode, the scan rate of CV measurement, the number of electrons appearing in half-reaction for the redox couple (n = 1),

the Faraday constant, the ideal gas constant and the absolute temperature, respectively. I_p is the anodic peak current.

The heterogeneous electron transfer rate (k_s) between the electrode and electrolyte in CV measurement, was calculated by the modified Kochi's expression as given in the Eq. S3[3,4].

$$k_s = (2.18)\left(\frac{\alpha DnF\nu}{RT}\right)^{1/2} exp\left[\frac{-\alpha^2 nF}{RT}\Delta E\right] \quad \text{(S3)}$$

where α is the transfer coefficient (0.5), D is the diffusion coefficient and ΔE represents the peak-to-peak separation voltage (ΔE = Epa–Epc; Epa and Epc are the anodic and cathodic peak potentials, respectively.

Electrode	Peak Current *Ip* (μA)	Diffusion coefficient D (cm^2/s)	Surface concentration I* ($mole/cm^2$)	Heterogeneous electron transfer rate K_s (cm/s)
RGO	669	34.37×10^{-2}	5.97×10^{-6}	15.0×10^{-2}
Cys	299.3	6.87×10^{-2}	2.66×10^{-6}	9.7×10^{-2}
Cys-RGO	438.2	14.73×10^{-2}	3.91×10^{-6}	12.85×10^{-2}
cMAb/Cys-RGO	228.4	4.1×10^{-2}	2.03×10^{-6}	1.68×10^{-2}

Table S1. Electrochemical parameters of various fabricated electrodes.

Electrochemical impedance spectroscopy (EIS) studies

The electrochemical impedance can be described either by the modulus $|Z|$ and the phase shift ϕ or by its real (Z′) and imaginary (Z″). The impedance is represented as a complex number,

$$Z(\omega) = \frac{E}{I} = Z_0\, exp(i\varphi) = Z_0\,(\cos\varphi + j\sin\varphi) \quad \text{(S4)}$$

The Randles circuit was used to determine the impedance containing an active electrolyte resistance R_S in series with charge transfer resistance R_{ct} the parallel arrangement of the double-layer capacitance C_{dl} or constant phase element (CPE) of a faradaic reaction (Fig. S4a, inset). A typical shape of Nyquist plot contains a semicircle region lying on the real axis followed by a straight line. The linear part ($\psi = \pi/4$), observed in the low frequency range, suggests a mass-transfer limited process, while the semicircle portion, observed in the high frequency range, indicates a charge-transfer limited process (Fig. S4a). Interfacial R_{ct} and C_{dl} in the Nyquist plot of impedance are found from real (Z') and imaginary ($-Z''$) impedance at different frequencies. The frequency related with maximum $-Z''$ and R_{ct} can be used to calculate C_{dl} using Eq. S5[5,6].

$$\frac{1}{2\pi f_{max}} = R_{ct}\, C_{dl} = \tau \qquad \text{(S5)}$$

where τ is the time constant and f_{max} is the maximum frequency.

The interfacial properties of electrodes were tested by calculating the charge transfer resistance (R_{ct}) and double layer capacitance (C_{dl}) at the conductive electrode and the electrolyte interface (Fig. S4a and b). R_{ct} is the diameter of semicircle portion in the impedance spectra, semicircle portion resembles to the finite process of electron transfer kinetics of redox study at the interface of a conductive electrode. Dielectric and insulating nature of materials can result in change in R_{ct} at the electrode/electrolyte interface.

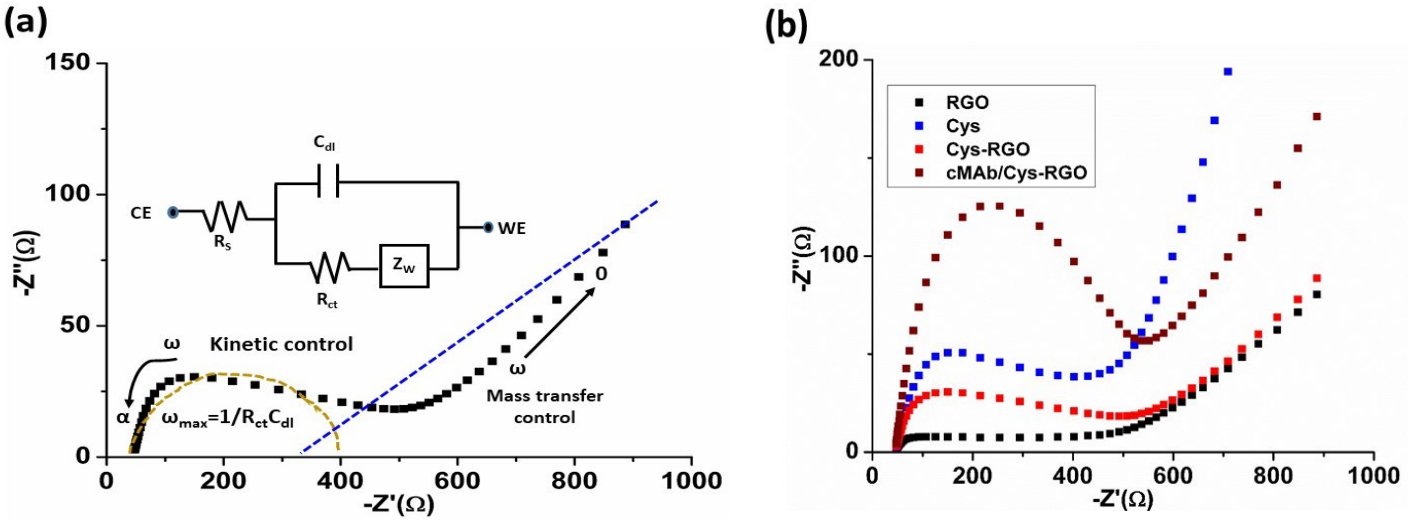

Fig. S4 (a) Nyquist plot and corresponded fitting for the Cys-RGO electrode by the EIS method to determine R_{ct} and C_{dl} values. (b) EIS spectra of RGO, Cys, Cys-RGO and cMAb/Cys-RGO.

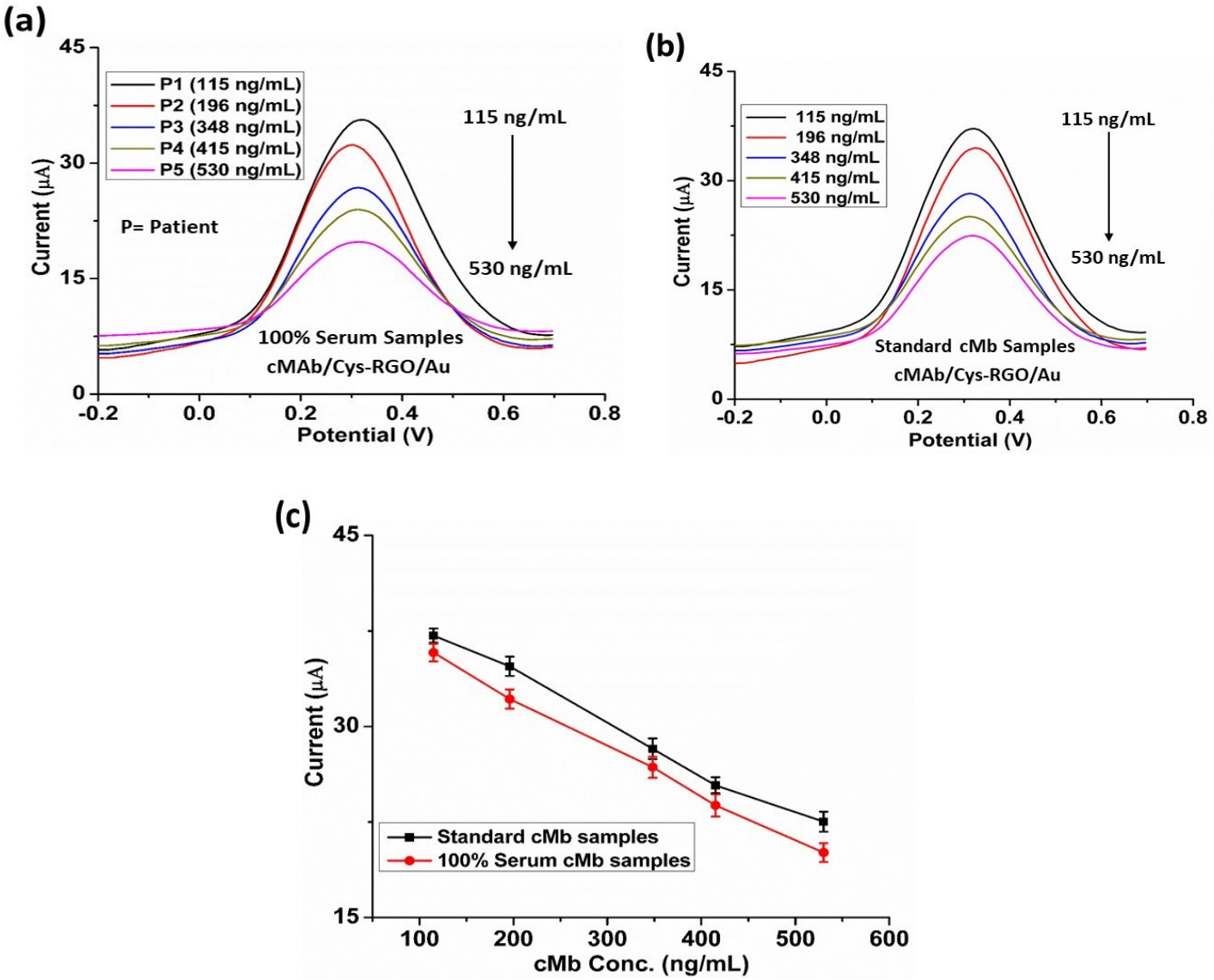

Fig. S5. (a) DPV response of the microfluidic device in presence of 100 % serum cMb of five cardiac patients (115–530 ng mL^{-1}). (b) DPV response of the device in presence of standard cMb samples (115–530 ng mL^{-1}). (c) Curves for DPV response current of the sensor answering to standard cMb samples and human serums of cMb. The relative standard deviation (%RSD) for all concentrations were determined of three repeated measurements with error bars.

S.No	cMb Conc. (ng mL^{-1})	Peak current (µA) obtained for standard cMb sample	Peak current (µA) obtained for 100% serum cMb sample	% Coefficient of variation for standard sample (N=3)	% Coefficient of variation for 100% serum sample (N=3)	Recovery (%)
1	115	37.13	35.8	2.52	3.98	96.42
2	196	34.72	32.15	4.93	5.24	92.61
3	348	28.25	26.8	6.91	7.57	94.87
4	415	25.38	23.8	4.65	8.92	93.78
5	530	22.52	20.26	8.1	7.97	89.96

Table S2. Determination of recovery and intra-assay coefficient of variation between peak current (µA) obtained for synthetic (standard) and 100% serum sample of cMb for different concentration using cMAb/Cys-RGO/Au sensor.

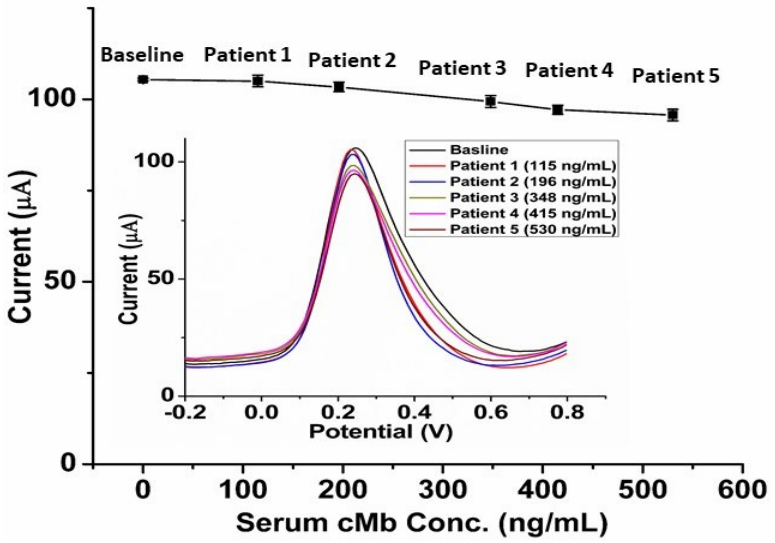

Fig. S6. Control experiment using Cys-RGO/Au electrode without incorporating antibody in presence of 100% serum spiked of five cardiac patients (115, 196, 348, 415 and 530 ng mL^{-1}). Inset shows the DPV response curves.

References

1 A. J. Bard, L. R. Faulkner, J. Leddy and C. G. Zoski, *Electrochemical methods: fundamentals and applications*, wiley New York, 1980, vol. 2.

2 R. Sharma, Md. A. Ali, N. R. Selvi, V. N. Singh, R. K. Sinha and V. V. Agrawal, *J. Phys. Chem. C*, 2014, **118**, 6261–6271.

3 R. J. Klingler and J. K. Kochi, *J. Am. Chem. Soc.*, 1980, **102**, 4790–4798.

4 M. Velický, D. F. Bradley, A. J. Cooper, E. W. Hill, I. A. Kinloch, A. Mishchenko, K. S. Novoselov, H. V. Patten, P. S. Toth, A. T. Valota, S. D. Worrall and R. A. W. Dryfe, *ACS Nano*, 2014, **8**, 10089–10100.

5 A. Kaushik, P. R. Solanki, K. Kaneto, C. G. Kim, S. Ahmad and B. D. Malhotra, *Electroanalysis*, 2010, **22**, 1045–1055.

6 Md. A. Ali, H. Jiang, N. K. Mahal, R. J. Weber, R. Kumar, M. J. Castellano and L. Dong, *Sens. Actuators B Chem.*, 2017, **239**, 1289–1299.